Reorganization of Alpha-Actinin and Vinculin Induced by a Phorbol Ester in Living Cells

James B. Meigs* and Yu-Li Wang*‡

*Department of Molecular and Cellular Biology, National Jewish Hospital and Research Center, Denver, Colorado 80206; and ‡Department of Biochemistry, Biophysics, and Genetics, University of Colorado Health Sciences Center, Denver, Colorado 80220

Abstract. We have used fluorescent analogue cytochemistry, image intensification, and digital image processing to examine the redistribution of alpha-actinin and vinculin in living cultured African green monkey kidney (BSC-1) cells treated with the phorbol ester 12-O-tetradecanoylphorbol-13-acetate (TPA). Before treatment, microinjected alpha-actinin shows characteristic distribution along stress fibers and at adhesion plaques; vinculin is localized predominantly at adhesion plaques. Soon after the addition of TPA, highly dynamic membrane ruffles begin to form. These incorporate a large amount of alpha-actinin but little vinculin. Alpha-actinin is subsequently depleted, more or less uniformly, from stress fibers. Disrupted stress fibers often fragment into aggregates and move into the perinuclear region. Careful analyses of fluorescence intensity distribution indicate that alpha-actinin is depleted more rapidly from adhesion plaques than from stress fibers. Furthermore, the depletion of alpha-actinin from adhesion plaques is also faster than either the depletion of vinculin or the disappearance of focal contacts. These observations indicate that TPA may initiate disruption of stress fibers by interfering with a link between alpha-actinin and vinculin, causing alpha-actinin to be preferentially depleted from adhesion plaques.

MANY cultured nonmuscle cells contain a well-organized set of stress fibers, which are large bundles of actin filaments associated with various accessory proteins such as alpha-actinin, myosin, and tropomyosin (for a review see reference 22). One of the most consistent characteristics of cells infected with transforming viruses, cells treated with tumor-promoting phorbol esters, and cells stimulated with growth factors, is the disorganization of stress fibers (for a review see reference 33). Since all of these agents stimulate various kinds of protein kinases (6, 8, 9, 12, 17, 25), it is possible that a common pathway is followed during the disruption process.

The reorganization of actin and vinculin induced by the tumor-promoting phorbol ester, 12-O-tetradecanoylphorbol-13-acetate (TPA),[1] has recently been studied using fluorescent phalloidin staining, immunofluorescence, and electron microscopy. Shortly after treatment, large actin-containing ruffles appear and stress fibers start to disappear from the cytoplasm (26, 30). Vinculin can be detected at the ends of stress fibers, where adhesion plaques are located, during the early stage of disruption. At steady state, the cell contains prominent ruffles and numerous aggregates of actin and vinculin. Although these studies have shown the dramatic effects of TPA, the actual process of structural reorganization can only be speculated upon since most observations were performed on different, fixed cells. In particular, it is not clear how the ruffles are related to disintegrating stress fibers, how the aggregates of actin are formed, whether the disassembly of stress fibers occurs with a specific directionality, and how the redistribution of vinculin relates to that of other components at adhesion plaques and along stress fibers.

It is clear that in order to reach a better understanding of the disruption of cellular structures and morphology, some experiments have to be performed on single living cells. In this study, we have used fluorescent analogue cytochemistry (32) to analyze the distributions of fluorescently labeled alpha-actinin and vinculin microinjected into living cells through the course of TPA treatment. To avoid light-induced cell damage and bleaching of the fluorophore, we have used extremely low levels of illumination in combination with a highly sensitive image intensifier. The image is processed by a digital image processing system, which provides not only high quality fluorescence images, but also quantitative information about the distribution of injected components. Our data indicate that stress fibers disintegrate in a nondirectional fashion into discrete aggregates, without a direct relationship to the formation of neighboring ruffles. In addition, we demonstrate that the depletion of alpha-actinin from adhesion plaques represents one of the earliest events during the disintegration of stress fibers.

[1] *Abbreviations used in this paper:* DMSO, dimethyl sulfoxide; FITC, fluorescein isothiocyanate; IATR, iodoacetamidotetramethylrhodamine; IRM, interference reflection microscopy; 4-alpha-PDD, 4-alpha-phorbol 12,13-didecanoate; TPA, 12-O-tetradecanoylphorbol-13-acetate.

Materials and Methods

Preparation of Fluorescent Analogues

Smooth muscle alpha-actinin was isolated from frozen chicken gizzards (Pel-Freez Biologicals, Rogers, AR) according to Feramisco and Burridge (15) with the following modification: after elution from a DE-52 column, fractions containing alpha-actinin were pooled and fractionated with a hydroxyapatite column (DNA-grade, Bio-Gel HTP, Bio-Rad Laboratories, Richmond, CA) before further fractionation with a Sepharose 6B-CL column (Sigma Chemical Co., St. Louis, MO). Purified alpha-actinin was concentrated by precipitation with solid ammonium sulfate, dialyzed exhaustively against 2 mM Pipes, 0.02% NaN_3, pH 7.0, and stored in liquid nitrogen at 13–15 mg/ml.

Smooth muscle vinculin was isolated from frozen chicken gizzards according to Evans et al. (13). Purified vinculin was concentrated and dialyzed as for alpha-actinin but was stored on ice at 4–5 mg/ml.

Labeling of alpha-actinin and vinculin with tetramethylrhodamine was performed by dissolving iodoacetamidotetramethyl rhodamine (IATR) (Research Organics, Cleveland, OH, or Molecular Probes, Inc., Junction City, OR) in 200 mM potassium borate buffer, pH 9.0. The solution was clarified in a Beckman type 42.2 Ti rotor at 100,000 *g* for 20 min to remove undissolved dye aggregates. Stored alpha-actinin or vinculin was mixed 1:1 (vol/vol) with the clarified dye solution. The molar ratio between the dye prior to clarification and the protein was 15 to 25 for alpha-actinin and 20 to 40 for vinculin. After mixing, the solution was incubated at 0°C for 4 h, clarified, and applied to a 0.7 × 15 cm column of Bio-Beads SM-2 (Bio-Rad Laboratories) to remove unbound dye molecules. The conjugate was eluted with 2 mM Tris-HCl, 0.1 mM dithiothreitol, pH 8.5. Fluorescent fractions in the void volume were pooled, concentrated with a Centricon-30 device (Amicon Corp., Danvers, MA), and dialyzed against injection buffer containing 1 mM Pipes, 0.1 mM dithiothreitol, pH 6.95. The alpha-actinin conjugate had a final concentration of 5 mg/ml and a final dye to protein subunit (100,000 dalton) molar ratio of 1.9 to 2.2 estimated using a molar extinction coefficient of 23,000 at 555 nm for bound tetramethylrhodamine. The vinculin conjugate had a final concentration of 1.3 to 10 mg/ml and a final dye to protein molar ratio of 0.50 to 0.75. The range of concentrations and labeling ratios did not affect our results.

Vinculin was labeled with fluorescein isothiocyanate (FITC) (Research Organics) by dissolving the dye in 200 mM potassium borate buffer, pH 9.0, and mixing 1:1 (vol/vol) with purified vinculin at an initial dye to protein molar ratio of 20. The solution was incubated at 0°C for 4 h, applied to a 1 × 15 cm column of Sephadex G-25 (Sigma Chemical Co.), and eluted with 2 mM Tris-Cl, 0.1 mM dithiothreitol, pH 8.5, to remove unbound dye molecules. Fluorescent fractions were pooled, concentrated to 3.7 mg/ml, and dialyzed against injection buffer. The conjugate had a final dye to protein molar ratio of 2.9 estimated using an extinction coefficient of 60,000 at pH 8.0 and 495 nm for bound fluorescein. FITC vinculin was co-injected with IATR alpha-actinin by mixing the two solutions 1:1 (vol/vol) before microinjection. Tetramethylrhodamine isothiocyanate-labeled (Research Organics) ovalbumin was prepared in a similar fashion to that previously described (35).

All conjugates were stored for up to a month on ice and were clarified at 100,000 *g* for 20 min before microinjection. The purity of the proteins and the absence of unbound dye were determined by SDS gel electrophoresis. The ability of the alpha-actinin conjugate to cross-link actin filaments was determined by falling-ball viscometry (21). Labeled alpha-actinin retained 100% of the cross-linking activity of the unlabeled protein.

Cell Culture, Microinjection, and Microscopy

African green monkey kidney cells (BSC-1; obtained from Dr. J. R. McIntosh, Department of Molecular Cell/Developmental Biology, University of Colorado, Boulder, CO) were cultured in Eagle's minimal essential medium (GIBCO, Grand Island, NY) supplemented with 10% fetal calf serum (KC Biological, Lenexa, KS), 50 U/ml penicillin, and 50 μg/ml streptomycin. Cells were plated onto coverslips 24–48 h before an experiment to <50% confluence and were microinjected as described previously (36). The injected volume of protein was estimated to be 2–5% of the cell volume. After microinjection, cells were incubated for at least 3 h to allow incorporation of injected analogues into cellular structures.

During observation, cells were maintained on a Zeiss IM-35 inverted microscope in humid air supplemented with CO_2 at a temperature of 31–32°C. Fluorescence images were observed with either a 63×/N.A. 1.25 neofluar phase objective or a 40×/N.A. 1.0 apochromatic objective, using epi-illumination with a 100-W quartz-halogen lamp operated at 6 V or less. To avoid crossover of rhodamine fluorescence into the fluorescein image during comparison of the two fluorophores, an additional barrier filter (cutoff wavelength, 550 nm) was added to the fluorescein filter set. Interference reflection microscopy (IRM) was performed with an epi-illuminator, a fluorescein filter set without the barrier filter, and an aperture inserted near the dichromatic mirror. The 485-nm bandpass filter in the light path minimized excitation and photobleaching of rhodamine-conjugated molecules.

Before treatment, a corresponding pair of rhodamine fluorescence and IRM, or rhodamine and fluorescein fluorescence images were obtained. TPA or 4-alpha-phorbol 12,13-didecanoate (4-alpha-PDD), dissolved in dimethyl sulfoxide (DMSO) (all from Sigma Chemical Co.) at a concentration of 1 mg/ml, was added to the culture dish on the microscope stage to a final concentration of 100 ng/ml. Pairs of images were subsequently recorded at 10-min intervals for up to 2 h.

Phallotoxin and indirect immunofluorescence staining were performed as described by Amato et al. (1). Fluorescein phalloidin was obtained from Molecular Probes, Inc. Rabbit anti-beef heart alpha-actinin and guinea pig anti-chicken gizzard vinculin were a kind gift of Dr. K. Burridge. Fluorescein goat anti-rabbit and fluorescein goat anti-guinea pig antibodies were obtained from Cappel Laboratories (Malvern, PA).

Image Recording and Processing

Images were detected using a Dage-MTI (Michigan City, IN) ISIT image intensifier coupled to an image processing system comprised of a DEC PDP 11/73 microcomputer, a 330-megabyte hard disk, image processing boards (three frame buffers, arithmetic logic unit, and analog processor; Imaging Technology Inc., Woburn, MA), and a graphics tablet (GTCO, Rockville, MD). The hardware was assembled by G. W. Hannaway and Associates (Boulder, CO); the image processing software was developed by G. W. Hannaway and Associates and by the authors.

During an experiment, raw images were fed from the image intensifier into the image processing system, which averaged 128 successive frames and stored the averaged image on the hard disk. Image averaging dramatically improved resolution and signal-to-noise ratio, yielding high-quality images even at extremely low levels of illumination. The gain and high-voltage settings on the image intensifier were kept constant, and the gamma correction circuitry was disabled for all experiments. The image intensifier has a linearity better than 95% over the range of operation.

For photography, an image of the dark-current was subtracted from each fluorescence image to remove background. Images were photographed from a video monitor on Tri-X film which was then developed in Diafine. For quantitative analysis, images were recalled and the background subtracted. Areas to be measured were delimited using a graphics tablet. The average fluorescence intensity in the delimited area was determined by dividing the integrated intensity by the number of pixels. Accumulation of molecules at adhesion plaques was expressed in terms of the ratio between the average fluorescence in an adhesion plaque to that in the surrounding cytoplasm. Thus any photobleaching during observation was normalized and values from different cells could be directly compared. The boundary of each adhesion plaque was determined based on the image before treatment. The same set of boundaries were used in a given cell at each subsequent time point. Thus any measured change in fluorescence signal represents a change over a constant area. Only adhesion plaques that were identifiable in corresponding IRM images through the course of measurement (~95% of all adhesion plaques in a given cell) were analyzed. Essentially the same technique was used to determine the ratio of average adhesion plaque fluorescence intensity to average associated stress fiber fluorescence intensity.

Results

Within 3 h after microinjection into BSC-1 cells (an epithelial cell line from African green monkey kidney), IATR alpha-actinin showed characteristic distribution along the length of stress fibers and at adhesion plaques, as described previously (14, 20). Microinjected IATR vinculin and FITC vinculin became incorporated primarily at adhesion plaques, also as previously reported (5, 16). We detected no difference in the pattern of incorporation between the IATR and FITC conjugates of vinculin.

The time course and specific details of morphological changes in response to TPA were apparently affected by the size of the cell. To reduce the range of variation, only cells between 50 and 100 μm in diameter will be considered here. The responses were in general similar to those described

previously (3, 11, 26, 30). The somewhat slower rate of change may be related to the lower temperature used here. None of the effects described below for TPA were observed with DMSO, 4-alpha-PDD, or medium alone. We have also processed cells microinjected with IATR alpha-actinin or IATR vinculin for indirect immunofluorescence using fluorescein-conjugated secondary antibodies. There invariably was a high degree of correlation, indicating that the microinjected conjugates were reliable indicators of the distribution of endogenous counterparts, at least at this level of resolution.

Formation of Membrane Ruffles and Disintegration of Stress Fibers

The most immediate change in BSC-1 cells after treatment with TPA was a dramatic increase in membranous ruffle-like structures (hereafter referred to as ruffles), which contained a large amount of injected IATR alpha-actinin (Figs. 1 *d* and 2 *b*, asterisks). These ruffles were dynamic, transient structures. Once formed, they could change shape, move laterally, or disappear within 2–10 min (Figs. 1 and 2). Since microinjected tetramethylrhodamine isothiocyanate–labeled ovalbumin did not concentrate in TPA-induced ruffles (not shown), the high fluorescence intensity of IATR alpha-actinin was probably not a result of high accessible volume. In addition, microinjected IATR vinculin entered ruffles to a much smaller extent than did IATR alpha-actinin. The difference between alpha-actinin and vinculin was clear in cells co-injected with IATR alpha-actinin and FITC vinculin (see Fig. 7).

Stress fibers lost alpha-actinin across their entire length

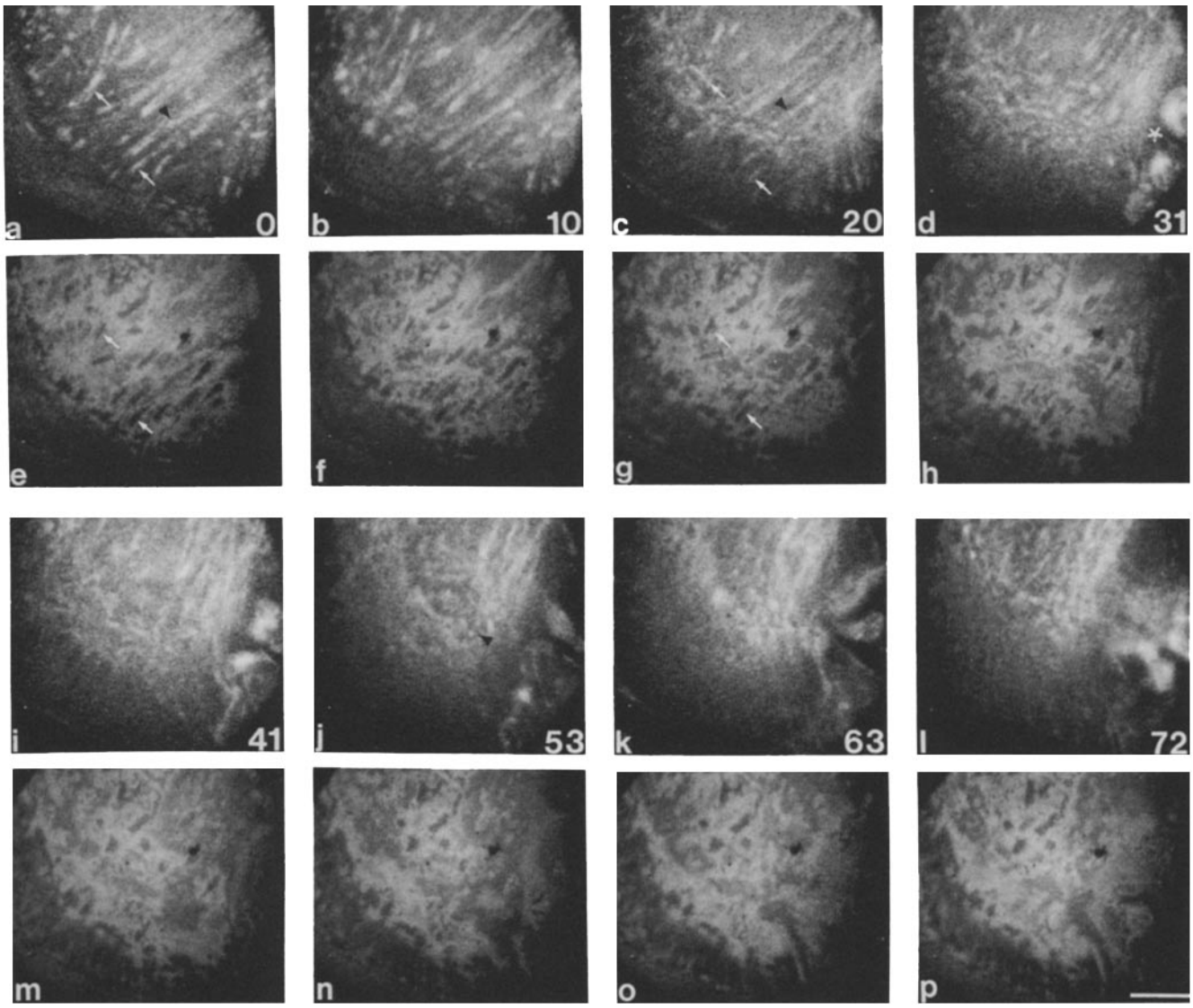

Figure 1. Time-lapse sequence of an IATR alpha-actinin–injected BSC-1 cell which is subsequently treated with 100 ng/ml TPA at t = 0. Fluorescence images are shown in upper photographs and the corresponding IRM images shown in lower photographs. Alpha-actinin appears to deplete rapidly from most adhesion plaques within 20 min (*a, c, e,* and *g*; arrows) and more slowly from associated stress fibers (*a* and *c*; arrowheads). Most adhesion plaques can be identified in the IRM images long after the depletion of alpha-actinin. Depletion of alpha-actinin from stress fibers appears to be uniform along the length. The stress fibers later move into the perinuclear region and form a network-like structure with alpha-actinin enriched at the foci (*j*; arrowhead). Some of the stress fibers fragment into small bundles. A bright fluorescent ruffle forms (*d*; asterisk) and subsequently disappears. Minutes after TPA treatment are indicated in the lower right corner of each fluorescence micrograph. Bar, 10 μm.

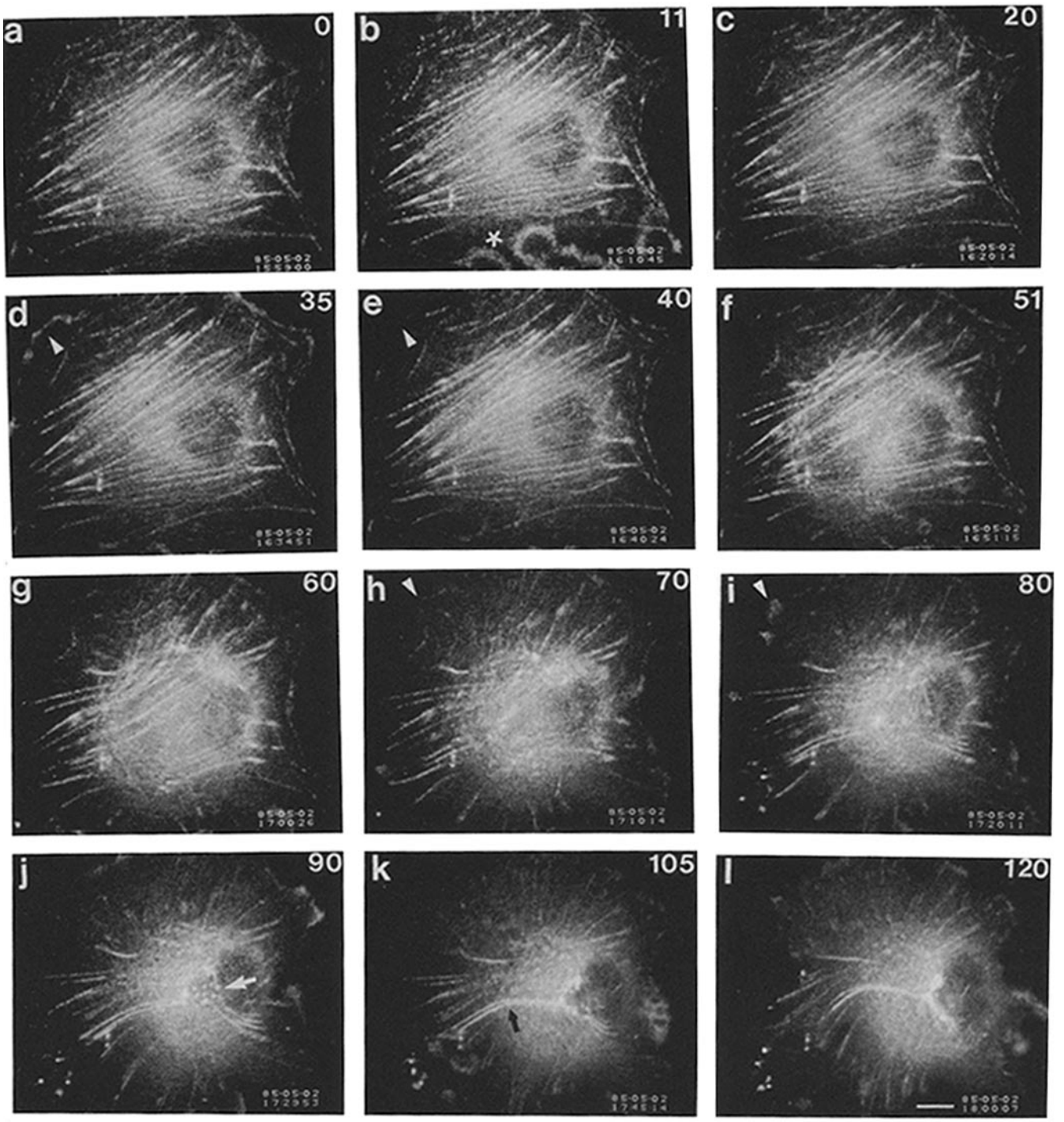

Figure 2. Time-lapse sequence of an IATR alpha-actinin–injected BSC-1 cell which is subsequently treated with 100 ng/ml TPA at t = 0. Several ring-shaped ruffles appear within 11 min after treatment (*b*; asterisk) and disappear by 20 min (*c*). Smaller ruffles later appear and disappear around the periphery (*d, e, h,* and *i*; arrowheads). At 51 min (*f*), peripheral stress fibers begin to move towards the nucleus. Over the next 30 min, these fibers become incorporated into a perinuclear network-like structure, with alpha-actinin enriched at the foci (*j*; white arrow). Some fibers become curved during the movement (*k*; black arrow). By 120 min (*l*) the cell has assumed a highly irregular morphology. Alpha-actinin aggregates and contorted fibers litter the cytoplasm. Minutes after TPA treatment are indicated in the upper right corner of each micrograph. Bar, 10 μm.

(Fig. 1 *c*, arrowheads) and frequently became fragmented into short bundles and aggregates (Figs. 1 and 2). In no case was depletion observed to proceed from one end of a fiber toward the other, or from the center of a fiber toward either end. In addition, there did not seem to be any direct temporal or spatial relationship between the formation of ruffles and the dissolution or reorganization of stress fibers.

Disintegrating stress fibers often moved into the perinuclear region (Figs. 1 and 2). Sometimes the fibers became curved as if they were pulled at a specific point in a direction

perpendicular to the axis of the fiber (Fig. 2*k*). In 20–30% of cells observed, a perinuclear network-like structure can be detected with alpha-actinin enriched at the foci (Fig. 1*j*, arrowhead, and Fig. 2*j*, white arrow). These networks eventually dispersed or disintegrated into random aggregates.

We have stained IATR alpha-actinin–injected cells with fluorescein–phalloidin to examine the distribution of actin filaments. Except for the more punctate appearance of alpha-actinin along stress fibers, there was a high degree of correlation between the rhodamine alpha-actinin and fluorescein–phalloidin images in both untreated and treated cells (Fig. 3). This suggests that the distribution of alpha-actinin can also be used as a close indicator of the distribution of actin filaments.

Alpha-actinin Is Depleted More Rapidly from Adhesion Plaques Than from Stress Fibers

In most cells examined, TPA appeared to induce a more rapid depletion of alpha-actinin from adhesion plaques than from stress fibers. For example, in the cell shown in Fig. 1*a*, adhesion plaques represented the most conspicuous structures before treatment, but diminished rapidly after the addition of TPA (Fig. 1*c*, arrows). A clear, high magnification view of this process is shown in Fig. 4, where alpha-actinin disappeared preferentially from adhesion plaques during the first 20 min of TPA treatment. Most focal contacts in the corresponding IRM image remained detectable long after alpha-actinin fluorescence had disappeared; they slowly lost their distinct shapes and darkness over a relatively long period of time (Figs. 1 and 4).

To quantify the relative loss of alpha-actinin from adhesion plaques and from stress fibers, we used digital image analysis to determine the ratio between the average fluorescence intensity of adhesion plaques (AP) and the average fluorescence intensity of associated stress fibers (SF). In untreated cells, the ratio AP/SF should be equal to or greater than one, as alpha-actinin is localized in both stress fibers and adhesion plaques but is enriched in adhesion plaques. If alpha-actinin is preferentially depleted from adhesion plaques after TPA treatment, then this ratio should decrease to a value less than one. This indeed was the case, as shown in Fig. 5. The ratio for control cells, on the other hand, remained larger than one over the same period of observation.

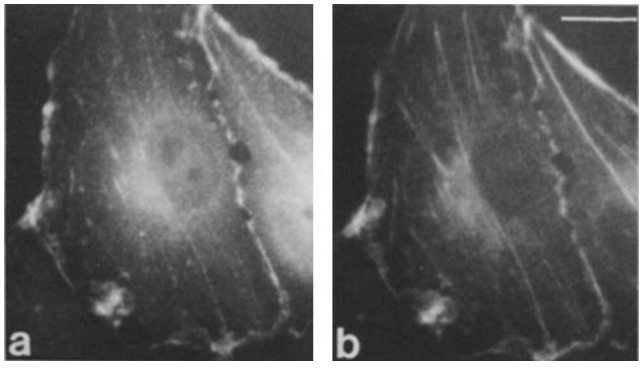

Figure 3. Close correlation between the distribution of injected IATR alpha-actinin and endogenous F-actin. A BSC-1 cell was microinjected with IATR alpha-actinin and subsequently treated with 100 ng/ml TPA for 30 min. The cell was fixed and stained with fluorescein phalloidin. (*a*) Fluorescence image of IATR alpha-actinin taken after fixation; (*b*) fluorescence image of fluorescein phalloidin. Except for the punctate appearance of alpha-actinin along stress fibers, there is a high degree of correlation between the two images. Bar, 10 μm.

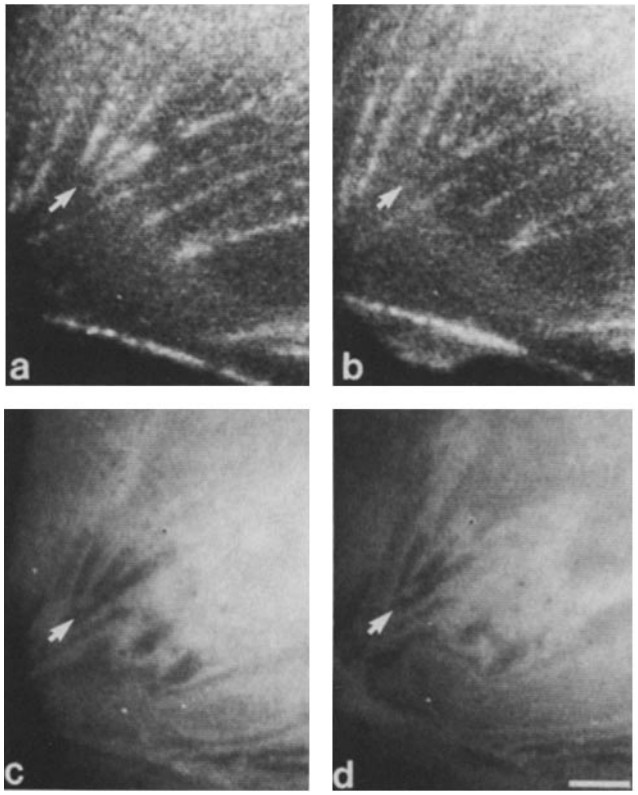

Figure 4. Rapid depletion of alpha-actinin from adhesion plaques. A BSC-1 cell was microinjected with IATR alpha-actinin. Fluorescence (*a*) and IRM (*c*) images before treatment with TPA show the presence of alpha-actinin along stress fibers and at adhesion plaques (arrow). 20 min after the addition of TPA, alpha-actinin disappears from adhesion plaques but remains associated with stress fibers (*b*). Substrate contacts also remain detectable (*d*). Bar, 5 μm.

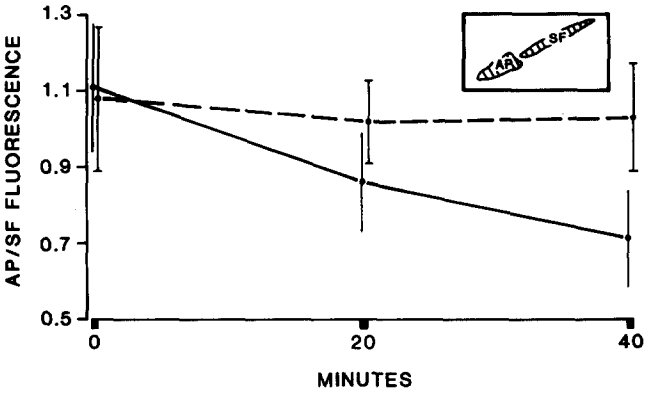

Figure 5. The ratio of IATR alpha-actinin average fluorescence intensity at adhesion plaques to that at associated stress fibers (AP/SF) as a function of time. TPA is added at t = 0 to cells previously microinjected with IATR alpha-actinin. The solid line shows average AP/SF for 25 adhesion plaques and their associated stress fibers in five cells. The dashed line shows average AP/SF for 15 adhesion plaques and stress fibers in three cells treated with either medium alone, DMSO, or 4-alpha-PDD. Vertical bars, ± 1 standard deviation. (*Inset*) Schematic diagram of the areas measured.

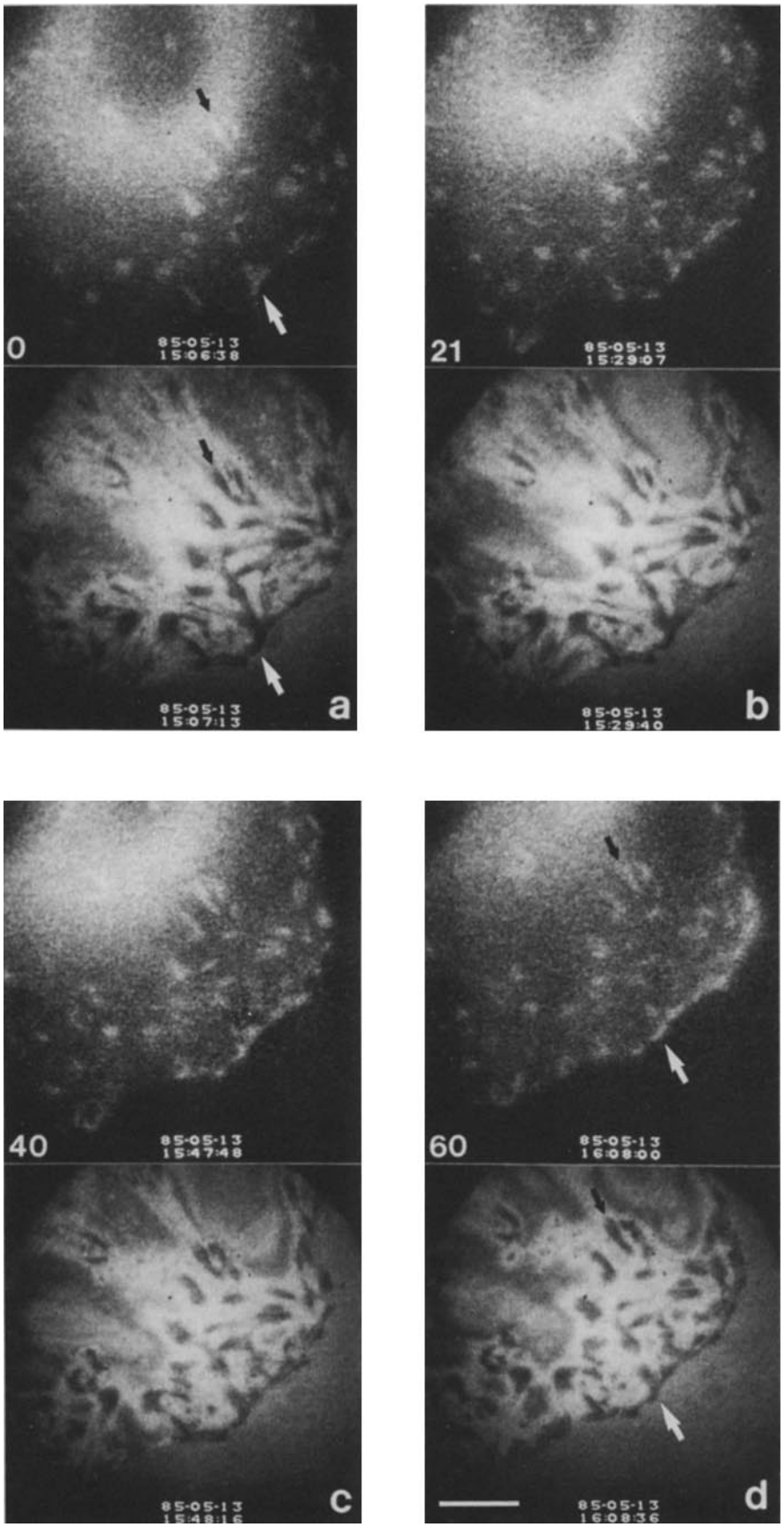

Figure 6. Time-lapse sequence of an IATR vinculin-injected BSC-1 cell which is subsequently treated with 100 ng/ml TPA at t = 0. Fluorescence images are shown in upper photographs and the corresponding IRM images shown in lower photographs. Vinculin fluorescence is diminished but still present in most adhesion plaques 60 min after treatment (*a* and *d*; arrows, upper photographs). Corresponding focal contacts also persist in the IRM image (*a* and *d*; arrows, lower photographs). Minutes after TPA treatment are indicated in the lower left corner of each fluorescence micrograph. Bar, 10 μm.

Alpha-actinin Is Depleted More Rapidly Than Vinculin from Adhesion Plaques

Since the dark focal contacts in IRM images remained detectable even long after IATR alpha-actinin fluorescence had disappeared from the corresponding adhesion plaques, we asked whether vinculin might remain in adhesion plaques longer than alpha-actinin. From Figs. 1 and 6, it appeared that microinjected IATR vinculin dissociated much more slowly from adhesion plaques than did alpha-actinin. Even after 60 min, all of the original adhesion plaques can still be identified in the fluorescent vinculin image. Staining of the cell in Fig. 6 with fluorescein-phalloidin indicated that most stress fibers indeed had been disrupted (not shown). In all cells injected with IATR vinculin, vinculin was present in adhesion plaques as long as they can be detected in the corresponding IRM images.

To quantify the loss of alpha-actinin or vinculin fluorescence from adhesion plaques, we measured the ratio of average adhesion plaque fluorescence (AP) to average adjacent cytoplasmic fluorescence (AC). If an adhesion plaque can be seen in a fluorescence image, the ratio AP/AC will be greater than one. If the adhesion plaque subsequently disappears this ratio will approach one. As shown in Table I, the mean ratio AP/AC for alpha-actinin decreased significantly after 40 min of TPA treatment. The mean ratio AP/AC for IATR vinculin, on the other hand, decreased only slightly within 60 min. The mean AP/AC for control cells decreased to some extent at 20 min, but remained constant thereafter. This decrease may be related to perturbations of the cells during the addition of solutions to the culture medium.

To demonstrate directly that alpha-actinin is depleted more rapidly than vinculin from adhesion plaques, we simultaneously microinjected IATR alpha-actinin and FITC vinculin into BSC-1 cells (Fig. 7). Before treatment, there was good correspondence between the two proteins at adhesion plaques. By 40 min after treatment, however, rhodamine fluorescence in most adhesion plaques has diminished considerably, while the corresponding fluorescein image showed little change.

Discussion

Although morphological alterations of cells treated with TPA have been studied previously by the use of phase-contrast, immunofluorescence, and electron microscopy (3, 11, 26, 30), the sequence of alteration remains uncertain. Fluorescent analogue cytochemistry allows us to follow dynamic processes directly in living cells and reach a more definitive understanding of the structural transformation process. The present study provides important information about how stress fibers disintegrate after TPA treatment, how the dissolution of stress fibers is related to the formation of ruffles and actin-contain-

Table I. Ratio of Average Fluorescence Intensities at Adhesion Plaques and in Adjacent Cytoplasm

	Time after addition of TPA or control solution			
	0	*20 min*	*40 min*	*60 min*
Alpha-actinin				
TPA-treated cells (110, 5)*	1.46 ± 0.16	1.24 ± 0.19	1.02 ± 0.13	—
Control cells (46, 3)	1.50 ± 0.14	1.29 ± 0.10	1.33 ± 0.15	1.29 ± 0.14
Vinculin				
TPA-treated cells (99, 5)	1.48 ± 0.18	1.37 ± 0.16	1.29 ± 0.16	1.20 ± 0.18
Control cells (48, 3)	1.42 ± 0.14	1.29 ± 0.09	1.34 ± 0.16	1.34 ± 0.17

Cells were microinjected with IATR alpha-actinin or IATR vinculin and incubated for at least 3 h. TPA dissolved in DMSO or an equal volume of control solution, which consisted of either medium, DMSO, or 4-alpha-PDD in DMSO, was then added at t = 0 min. Fluorescence intensities were then measured and ratios calculated at specified time points as described in Materials and Methods.

* Numbers indicate that data were collected from 110 adhesion plaques in 5 cells.

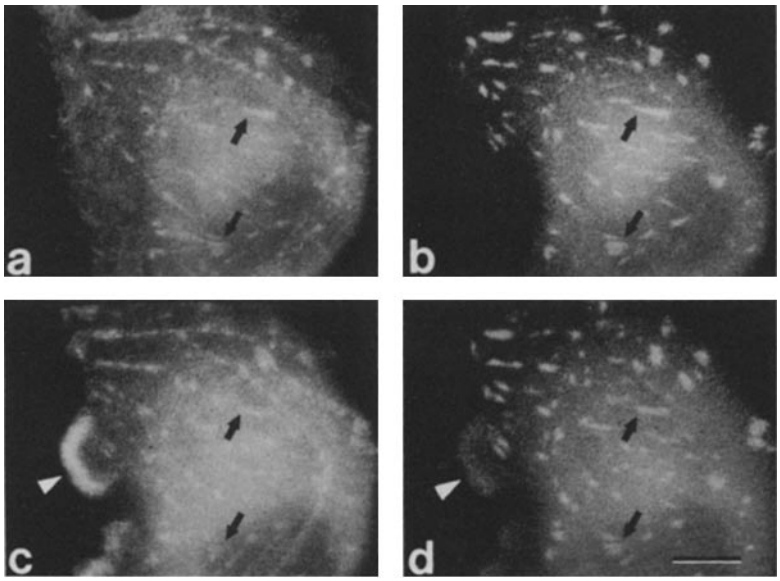

Figure 7. A BSC-1 cell coinjected with IATR alpha-actinin (*a* and *c*) and FITC vinculin (*b* and *d*). Fluorescence images are recorded before (*a* and *b*) and 40 min after (*c* and *d*) treatment with 100 ng/ml TPA. Alpha-actinin is significantly depleted from most adhesion plaques by this time (*a* and *c*; arrows); vinculin distribution remains relatively unchanged (*b* and *d*; arrows). A large ruffle forms which contains a large amount of alpha-actinin (*c*; arrowhead) but much less vinculin (*d*; arrowhead). Bar, 10 μm.

ing aggregates, and how the integrity of stress fibers is related to the association with adhesion plaques.

The structures induced most immediately by TPA are the highly dynamic ruffles, which, unlike ruffles in untreated cells, can appear close to stress fibers. However, although previous investigators have noted a strong coincidence between increased membrane ruffling and loss of stress fibers (2, 4, 24, 29, 34), we have never detected a direct temporal relationship between the disruption of a specific stress fiber and the appearance of ruffles in its vicinity. Thus it is unlikely that ruffles directly induce the breakdown of stress fibers.

TPA, however, may induce breakdown of stress fibers through disruption of adhesion plaques. The possible role of adhesion plaques and vinculin in the maintenance of the integrity of stress fibers has long been a subject of speculation (19). On the one hand, vinculin appears to co-localize with the transforming kinase, pp60^{src}, in cells infected with the Rous sarcoma virus (27), and is one of the primary components phosphorylated during viral transformation as well as during treatments of TPA and growth factors (12, 31, 37). The subsequent disruption of stress fibers suggests that vinculin and adhesion plaques may play a crucial role in their stability. On the other hand, the extent of vinculin phosphorylation seems limited in transformed cells (31), and increases in vinculin phosphorylation alone appears insufficient to cause dissolution of stress fibers (28).

Our results indicate that both adhesion plaques and associated vinculin persist even after most stress fibers have become disrupted. Therefore, it is unlikely that the disintegration of stress fibers is caused by the depletion of vinculin molecules or the detachment of substrate contact. Conversely, neither the maintenance of substrate contact nor the association of vinculin with adhesion plaques appears to be directly dependent on the association with stress fibers or the presence of alpha-actinin.

However, our data indicate that alpha-actinin at adhesion plaques may play an important role in the stability of stress fibers. The depletion of alpha-actinin from adhesion plaques represents one of the earliest events following TPA treatment. This was then followed by the dissociation of alpha-actinin (and presumably, other components, including actin) along the length of stress fibers as well as fragmentation of stress fibers. Many fibers subsequently move into the perinuclear region. Eventually the stress fibers disperse or disintegrate into numerous actin- and alpha-actinin–containing bundles and aggregates. Thus it is possible that the dissociation of alpha-actinin from adhesion plaques causes stress fibers to dissociate from adhesion plaques and subsequently disintegrate.

It will be very important to determine the mechanism involved in the rapid depletion of alpha-actinin from adhesion plaques. At adhesion plaques, vinculin is localized closer to the plasma membrane than alpha-actinin (7). TPA may interfere with a link between alpha-actinin and vinculin, causing alpha-actinin, but not vinculin, to dissociate from adhesion plaques. Alternatively, alpha-actinin may be depleted from adhesion plaques through competitive binding with ruffles, or through an alteration of the cytoplasmic ionic environment (10, 23).

Our results contrast with the recent report by Herman and Pledger (18) that vinculin redistribution is the primary event in microfilament reorganization induced by the platelet-derived growth factor. Although there is no clear explanation at present, the difference may reflect some subtle but important differences between the disruptions induced by various agents. For example, the different kinases activated by TPA and platelet-derived growth factor may have different effects on vinculin. In addition, the formation of ruffles is much more pronounced in cells treated with TPA than with platelet-derived growth factor (18, 30). Future applications of fluorescent analogue cytochemistry to cells treated with growth factors and cells infected with transforming viruses should shed light on the similarities as well as differences among these related processes.

We thank Dr. Keith Burridge for the generous gift of anti-alpha-actinin and anti-vinculin antibodies, Dr. J. Richard McIntosh for the gift of BSC-1 cells, and Dr. N. M. McKenna, C. S. Johnson, and S. Stickel for reading the manuscript.

This study was supported by American Cancer Society grant CD-200, National Science Foundation grant PCM-8306971, and a grant from the Muscular Dystrophy Association. The experiments were performed at the Doris W. Neustadt Laboratory of Cellular Structure at the National Jewish Hospital and Research Center.

Received for publication 1 July 1985, and in revised form 2 December 1985.

Note Added in Proof: Drs. Takahashi, Junker, and Heine at the National Cancer Institute informed us, through personal communication, of their observation that stress fibers in the epidermal cell line JB6 disappear more rapidly than vinculin plaques after TPA treatment.

References

1. Amato, P. A., E. R. Unanue, and D. L. Taylor. 1983. Distribution of actin in spreading macrophages: a comparative study on living and fixed cells. *J. Cell Biol.* 96:750–761.

2. Bloom, G. S., and A. H. Lockwood. 1980. Redistribution of myosin during morphological reversion of Chinese hamster ovary cells induced by db-cAMP. *Exp. Cell Res.* 129:31–45.

3. Boreiko, C., S. Mondal, K. S. Narayan, and C. Heidelberger. 1980. Effect of 12-O-tetradecanoylphorbol-13-acetate on the morphology and growth of C3H/10T1/2 mouse embryo cells. *Cancer Res.* 40:4709–4716.

4. Boschek, C. B., B. M. Jockush, R. R. Friis, R. Back, E. Grundmann, and H. Bauer. 1981. Early changes in the distribution and organization of microfilament proteins during cell transformation. *Cell.* 24:175–184.

5. Burridge, K., and J. R. Feramisco. 1980. Microinjection and localization of a 130K protein in living fibroblasts: a relationship to actin and fibronectin. *Cell.* 19:587–595.

6. Castanaga, M., Y. Takai, K. Kaibuchi, K. Sano, U. Kikkawa, and Y. Nishizuka. 1981. Direct activation of calcium activated, phospholipid-dependent protein kinase by tumor promoting phorbol esters. *J. Biol. Chem.* 257: 7847–7851.

7. Chen, W. T., and S. J. Singer. 1982. Immunoelectron microscopic studies of the sites of cell-substratum and cell-cell contacts in cultured fibroblasts. *J. Cell Biol.* 95:205–222.

8. Collet, M. S., A. F. Purchio, and R. L. Erikson. 1980. Avian sarcoma virus-transforming protein, pp60^{src}, shows protein kinase activity specific for tyrosine. *Nature (Lond.).* 285:167–169.

9. Cooper, J. A., D. F. Bowen-Pope, E. Raines, R. Ross, and T. Hunter. 1982. Similar effects of platelet-derived growth factor and epidermal growth factor on the phosphorylation of tyrosine in cellular proteins. *Cell.* 31:263–273.

10. Croop, J., G. Dubyak, Y. Toyama, A. Dlugosz, A. Scarpa, and H. Holtzer. 1982. Effects of 12-O-tetradecanoylphorbol-13-acetate on myofibril integrity and Ca^{++} content in developing myotubes. *Dev. Biol.* 89:460–474.

11. Driedger, P. F., and P. M. Blumberg. 1977. The effect of phorbol diesters on chicken embryo fibroblasts. *Cancer Res.* 37:3257–3265.

12. Ek, B., B. W. Westermark, A. Wasteson, and C.-H. Heldin. 1982. Stimulation of tyrosine-specific phosphorylation by platelet-derived growth factor. *Nature (Lond.).* 295:419–420.

13. Evans, R. R., R. M. Robson, and M. H. Stromer. 1984. Properties of smooth muscle vinculin. *J. Biol. Chem.* 259:3916–3924.

14. Feramisco, J. R. 1979. Microinjection of fluorescently labeled alpha-actinin into living fibroblasts. *Proc. Natl. Acad. Sci. USA.* 76:3967–3971.

15. Feramisco, J. R., and K. Burridge. 1980. A rapid purification of alpha-actinin, filamin, and a 130,000 dalton protein from smooth muscle. *J. Biol. Chem.* 255: 1194–1199.

16. Geiger, B. 1979. A 130K protein from chicken gizzard: its localization at the termini of microfilament bundles in cultured chicken cells. *Cell.* 18:193–205.

17. Gilmore, T., and G. S. Martin. 1983. Phorbol ester and diacylglycerol induce protein phosphorylation at tyrosine. *Nature (Lond.).* 306:487–490.

18. Herman, B., and W. J. Pledger. 1984. Platelet-derived growth factor–induced alterations in vinculin and actin distribution in BALB/c-3T3 cells. *J. Cell Biol.* 100:1031–1040.

19. Hynes, R. 1982. Phosphorylation of vinculin by pp60^{src}: what might it mean? *Cell.* 28:437–438.

20. Lazarides, E., and K. Burridge. 1975. Alpha-actinin: immunofluorescent localization of a muscle structural protein in nonmuscle cells. *Cell.* 6:289–298.

21. MacLean-Fletcher, S. D., and T. D. Pollard. 1980. Viscometric analysis of the gelation of acanthamoeba extracts and purification of two gelation factors. *J. Cell Biol.* 85:414–428.

22. Maness, P. F. 1981. Actin structure in fibroblasts—its possible role in transformation and tumorgenesis. *In* Cell and Muscle Motility, Vol. I. R. M. Dowben and J. W. Shaw, editors. Plenum Publishing Corp., New York. 335–373.

23. McNeil, P. L., M. McKenna, and D. L. Taylor. 1985. A transient rise in cytosolic calcium follows stimulation of quiescent cells with growth factors and is inhibitable with phorbol myristate acetate. *J. Cell Biol.* 101:372–379.

24. Mellstrom, K., A.-S. Hoglund, M. Nister, C.-H. Hedlin, B. Westermark, and U. Lindberg. 1983. The effect of platelet-derived growth factor on morphology and motility of human glial cells. *J. Muscle Res. Cell Motil.* 4:589–609.

25. Niedel, J. E., C. J. Kuhn, and G. R. Vanderbark. 1983. Phorbol diester receptor copurifies with protein kinase C. *Proc. Natl. Acad. Sci. USA.* 80:36–40.

26. Rifkin, D. B., R. M. Crowe, and R. Pollack. 1979. Tumor promoters induce changes in the chick embryo fibroblast cytoskeleton. *Cell.* 18:361–368.

27. Rohrschneider, L. R. 1980. Adhesion plaques of Rous sarcoma virus–transformed cells contains the src gene products. *Proc. Natl. Acad. Sci. USA.* 77:3514–3518.

28. Rohrschneider, L., and M. J. Rosok. 1983. Transformation parameters and pp60^{src} localization in cells infected with partial transformation mutants of Rous sarcoma virus. *Mol. Cell. Biol.* 3:731–746.

29. Schlessinger, J., and B. Geiger. 1981. Epidermal growth factor induces redistribution of actin and alpha-actinin in human epidermal carcinoma cells. *Exp. Cell Res.* 134:273–279.

30. Schliwa, M., T. Nakamura, K. R. Porter, and U. Euteneuer. 1984. A tumor promoter induces rapid and coordinated reorganization of actin and vinculin in cultured cells. *J. Cell Biol.* 99:1045–1059.

31. Sefton, B. M., T. Hunter, E. H. Ball, and S. J. Singer. 1981. Vinculin: a cytoskeletal target of the transforming protein of Rous sarcoma virus. *Cell.* 24:165–174.

32. Taylor, D. L., and Y.-L. Wang. 1978. Molecular cytochemistry: incorporation of fluorescently labeled actin into living cells. *Proc. Natl. Acad. Sci. USA.* 75:857–861.

33. Vasiliev, J. M. 1985. Spreading of non-transformed and transformed cells. *Biochim. Biophys. Acta.* 780:21–65.

34. Wang, E., and A. Goldberg. 1976. Changes in microfilament organization and surface topography upon transformation of chick embryo fibroblasts with Rous sarcoma virus. *Proc. Natl. Acad. Sci. USA.* 73:4065–4069.

35. Wang, Y.-L., and D. L. Taylor. 1979. Distribution of fluorescently labeled actin in living sea urchin eggs during early development. *J. Cell Biol.* 82:672–679.

36. Wang, Y.-L. 1984. Reorganization of actin filament bundles in living fibroblasts. *J. Cell Biol.* 99:1478–1485.

37. Werth, D. K., J. E. Niedel, and I. Pastan. 1983. Vinculin, a cytoskeletal substrate for protein kinase C. *J. Biol. Chem.* 258:11423–11426.